

Investigation of compositional analysis and physical properties for Ni-Cr-Nb alloys using laser-induced breakdown spectroscopy

HUSSEIN SALLOOM^{1*}, TAGREED HAMAD²

¹Al-Nahrain Nanorenewable Energy Center, Al-Nahrain University, Iraq

²Laser and Optoelectronics Department, College of Engineering, Al-Nahrain University, Iraq

*Corresponding author: abnthamer@gmail.com

In this work, laser-induced breakdown spectroscopy (LIBS) analysis is optimized for direct estimation of elemental composition, thermal conductivity and hardness for Ni-Cr-Nb alloys. These alloys were chosen with a variable elemental content of niobium and chromium. The influence of laser energy and shot numbers on measuring line intensity was investigated. Based on the ratio between two spectral lines, calibration curves were formed to estimate the element concentration and LIBS results were confirmed with related energy-dispersive X-ray spectroscopy (EDS) data. Hardness and thermal conductivity estimation using LIBS were done by measuring the ratio between two spectral lines, plasma excitation temperature and electron density for different samples. Semi-empirical formulas correlated hardness and thermal conductivity with plasma temperature were established.

Keywords: LIBS technique, elemental analysis, nickel alloys, hardness.

1. Introduction

As a kind of emission spectroscopy, laser-induced breakdown spectroscopy (LIBS) technology has been widely investigated and developed for variety of applications thanks to its unique and attractive features [1, 2]. Whilst qualitative and quantitative compositional analysis of geological [3], archaeological [4] and industrial [5] materials have taken the principal part in LIBS application, many other industrial applications witnessed quick progress. Concerned industrial applications include hazard pollution detection, raw material exploring, rapid sorting, depth profiling, hardness estimation and so on.

Many laboratory studies and industrial projects [6] addressed the analysis of metals and metallic alloys. KUZUYA [7] classified aluminum alloy scrap by checking the difference of the concentration of main additional elements (Si, Cu, Mn, Mg, and Zn) which was determined by the calibration curves. VARELA *et al.* [8] demonstrated the feasibility

of LIBS as a suitable analytical tool for characterizing NiCrBSi-WC coatings cladded by laser. KASHIWAKURA *et al.* [9] proposed a promising method to sort steel scrap precisely with relatively high Cu contents. ARARAT-IBARGUEN *et al.* [10] applied LIBS to investigate the rapid diffusion of impurities in Zr based alloys. GAUDIUSO *et al.* [11] acquired depth profiles at six spots of Sasanian metallic coins to determine the concentration of (Hg, Ag, Cu, Pb, Au, Si, Ca) elements. LI *et al.* [12] reported using LIBS to analyze T9 steel samples having various aging grades in order to predict the correlation between LIBS spectral analysis of steel and aging grade. WANG *et al.* [13] suggested the *in situ* LIBS based monitoring system correlating the intensity of emission lines with micro-hardness of AISI4140 steel molten zone. LEGNAIOLI *et al.* [14] presented a valuable and broad review related to industrial applications of LIBS. They focused on researches where LIBS analysis made big differences compared to other techniques. Also, they reported the novel developing applications including the sorting of metallic waste and selective plastic recycling.

Added to this, extensive efforts have been focused on the innovative idea of using LIBS technique for estimating hardness. The simple experimental set up with little sample preparation, non-contact analysis and easy data collection of LIBS make it a desirable tool for *in situ* hardness measurements. It is found that the intensity ratio of neutral to ionic spectral lines can be correlated with material strength [12, 15]. This correlation was attributed to the repulsive force of the laser-induced shockwaves. It was experimentally confirmed that the repulsion of the shock wave on the hard materials is much strong to produce a high-speed shock wave. Consequently, enough temperature is generated just behind the shock wave to ionize the atoms leading to an increase in ionic emission intensity in comparison with the intensity of neutral emission [16]. Moreover, studies revealed that the hardness of various materials can be evaluated by monitoring the plasma parameters, *i.e.* electron density and temperature [17]. This research aims to obtain precise elemental composition of Ni-Cr-Nb nickel alloys using laser-induced plasma (LIP) of niobium and chromium with respect to nickel. In addition, the relationship between the ratio of spectral lines with thermal conductivity and surface hardness of considered alloys was investigated. Moreover, plasma parameters have been employed to estimate thermal conductivity and surface hardness of considered alloys.

2. LIBS theory and principle

LIBS principle relies on three successive physical processes: laser-matter interaction, generation of micro-plasma and expansion of plasma and cooling. The first two processes start with the arrival of the laser pulse and continue until the duration of the laser pulse, whereas the last process starts after the ending of the laser pulse [18]. When one or more energetic laser pulses are focused on the sample surface, the laser energy is absorbed by the surface and converted into heat energy. During local heating, melting and intense evaporation, a small amount from the sample material will be ablated and plasma

plume of high-pressure is produced. During the plasma cooling, excited atoms and ions in the upper state will relax and come back to their ground state and thereupon radiative emissions of the light at representative wavelengths of the ablated target are observed. The laser induced plasma characteristics depend on several parameters including the material properties, laser parameters and the properties of the ambient medium. The maximum amount of material that could be vaporized M_v is related to the laser energy E and thermal properties of materials according to the following equation [18, 19]:

$$M_v = \frac{E(1 - R)}{C_p(T_b - T_0) + L_v} \quad (1)$$

where R , C_p , T_b , T_0 , L_v are surface reflectivity, specific heat, boiling temperature, initial temperature and latent heat of the material. The emission from the plasma gives the chemical compositional information of the target material. Supposing that the produced plasma is under local thermal equilibrium (LTE) conditions, the intensity I_k of an emission line (k) can be given by [18]:

$$I_k = C_i M_v \frac{g_k A_{k_i} h c}{Z \lambda_k} \exp(-E_k / k_B T) \quad (2)$$

where C_i is the concentration of the element i in the plasma, while g_k , A_{k_i} , E_k , Z , T are the statistical weight, the transition probability, the energy of the excited state, the partition function and the temperature, respectively. Therefore, the line intensity is directly proportional to the population densities of species presented in the plasma, that is, to the amount of vaporized material available for excitation M_v .

In addition to elemental analysis, plasma parameters such as excitation temperature T_e and electron number density N_e can be determined from the emission spectrum. For calculation of T_e , Eq. (2) requisites rearrange to establish the Boltzmann plot as given in the following expression [20]:

$$\ln\left(\frac{I}{g_k A_{k_i}}\right) = \frac{-E_k}{k_B T} + C \quad (3)$$

Here, the natural logarithm of rescaled intensities of selected emission lines was plotted *versus* the upper state energy (E_k) to result in a straight line with the slope of $(-1/k_B T)$. For electron number density N_e calculation, the Stark broadening of well resolved spectral lines can be used according to the relation [21, 22]:

$$N_e = \frac{\Delta \lambda_{\text{FWHM}}}{2 \omega_s} N_r \quad (4)$$

In Eq. (4), $\Delta \lambda$ is the Lorentzian FWHM of the spectral line, ω_s is the Stark broadening parameter, values of which can be found in scientific data tables, N_r is the reference

electron density equal to 10^{16} (cm^{-3}) for neutral atoms and 10^{17} (cm^{-3}) for singly ionized states.

3. Experimental part

3.1. Samples

Four kinds of (Ni-Cr-Nb) Ni-based alloys manufactured by vacuum arc-melting were used in this work. The nominal concentrations and composition of alloys were tested by energy dispersive spectroscopy (EDS) system (Model: EX23000 BU). The choice of these alloys was based on the variable concentrations of chromium and niobium with unchanged nickel. The tested result of sample No. 1 was shown in Fig. 1. The micro-hardness and thermal conductivity were measured using micro-hardness tester (model: HVS-1000Z) and Lee's Disc apparatus, respectively. The measured values are listed in Table 1.

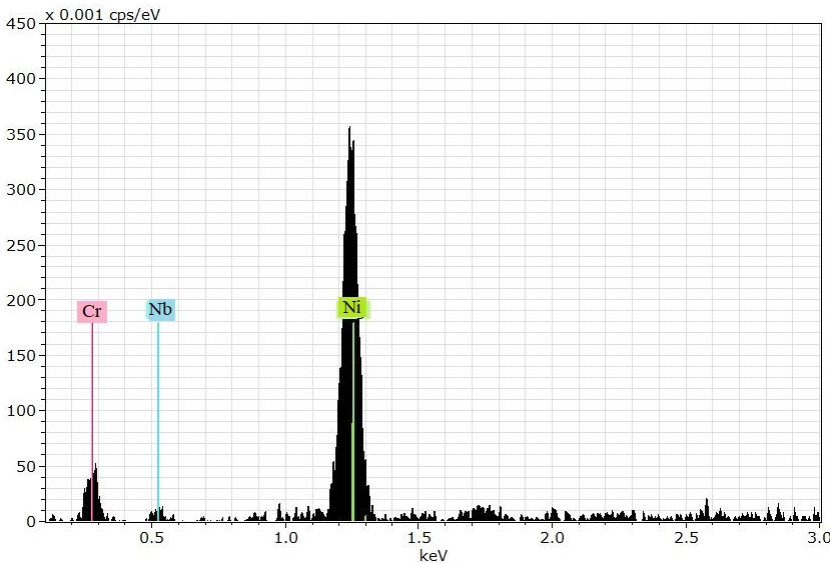


Fig. 1. EDS of sample No. 1 (Ni-24Cr-8Nb) alloy.

Table 1. Compositional analysis of Ni-Cr-Nb alloys measured by EDS analysis.

No.	Sample	Hardness	Thermal conductivity [W/m·k]
1	Ni-24Cr-8Nb	245	90
2	Ni-22Cr-10Nb	315	82
3	Ni-20Cr-12Nb	380	70
4	Ni-18Cr-14Nb	440	63

3.2. Reference materials

For quantitative purpose, calibration curves have been obtained using standard reference materials of (Ni-Cr) and (Ni-Nb). Elemental contents of these alloys are given in Table 2.

T a b l e 2. Contents of standard reference alloys used to obtain calibration curves.

No.	Cr [wt.%]	Nb [wt.%]	Ni [wt.%]
Ni-Cr	30	–	70
	25	–	75
	20	–	80
	18	–	82
	15	–	85
	12	–	88
Ni-Nb	–	19	81
	–	18	82
	–	15	85
	–	13	87
	–	11	89
	–	9	91
	–	5	95

3.3. Optical system

Lab built LIBS set up was designed and utilized to produce plasma by ablating Ni-Cr-Nb alloys target. A Q-switched Nd: YAG laser operating at a wavelength of 1064 nm and a pulse duration of 9 ns was used for the ablation process. The laser pulse energy was varied from 50 to 200 mJ to obtain different laser fluences for various numbers of laser pulses ranging from 1 to 50. Target was fixed on 3-D stage perpendicular to the laser beam. Plasma emission was detected using (Maya2000 Pro) spectrometer operating at 1.0 μ s gate delay and 1.0 ms integration time. Plasma emissions are collected via a multi-mode optical fiber cable with a diameter of 400 μ m. Identification of interested spectral lines was performed according to NIST atomic spectral database [23].

4. Result and discussion

4.1. Optimization of LIBS spectra

The spectra of Ni-Cr-Nb alloy in ambient air is shown in Fig. 2. The atomic and ionic lines of nickel, chromium and niobium having less interference and enough intensities have been identified [24]. These spectral lines for Ni, Cr and Nb were chosen to evaluate the composition analysis of four Ni-Cr-Nb alloys having different chemical com-

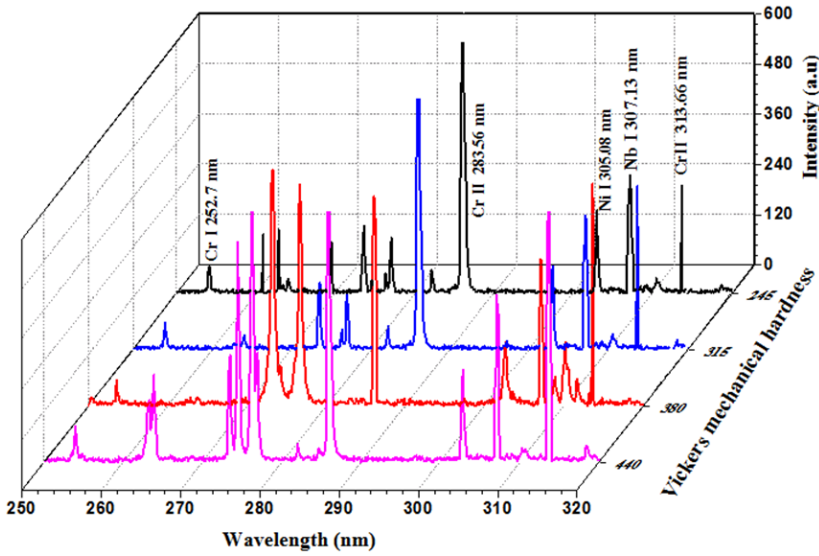


Fig. 2. Emission spectra for four examined nickel alloys having different Vickers hardness values.

positions. Also, the analysis of these spectra will be given in the following sections to study the correlation between plasma parameters and physical properties of examined alloys.

Optimizing procedures have been adopted by studying the influence of laser energy on emission lines intensities of sample No. 1 (Ni-24Cr-8Nb) alloy as shown in Fig. 3.

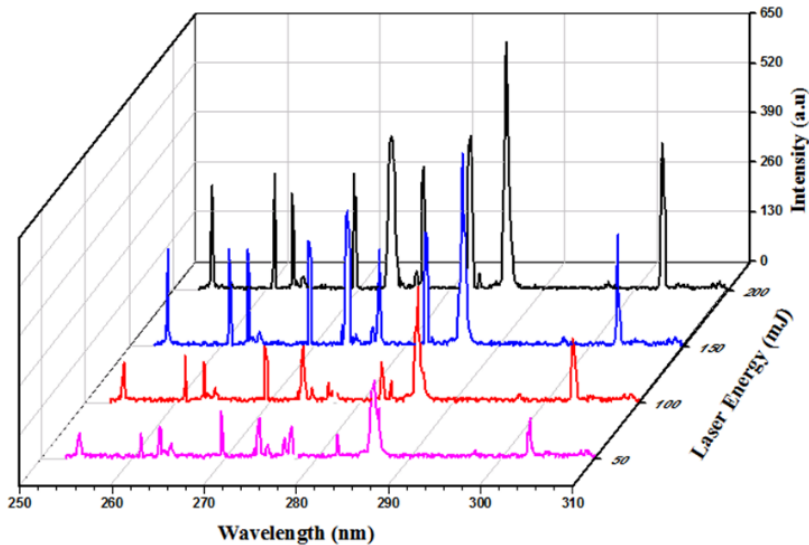


Fig. 3. Emission intensity of spectral lines of sample No. 1 at various laser energies ranging from 50 to 200 mJ.

It can be seen that there is a significant enhancement in the intensity of all identified lines as laser peak power increased from 50 to 200 mJ, due to higher mass ablation rate from the target and higher number of excited atoms leading to increased peak intensity of the emission lines. However, this increase is addressed by other related works [20, 25] and suffers from saturation effect, especially at thick optical plasma due to plasma shielding [26].

On the other hand, to enhance the quantitative analysis of samples, the accumulating energy of laser radiation and laser shots is usually used to get better signal intensity [27] and reduce signal fluctuations from pulse to pulse [28] during measurements. Herein, the relative standard deviation (RSD) of the measurements performed under the same

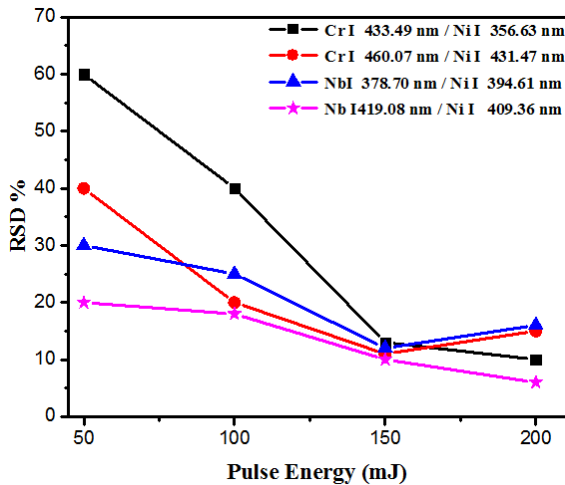


Fig. 4. RSD of the ratios Cr I/Ni II and Nb I/Ni II line of peak intensities *versus* laser pulse energy.

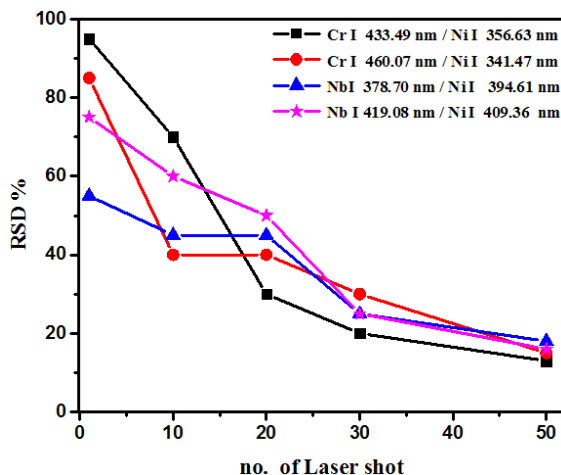


Fig. 5. RSD of the ratios of line intensities *versus* the number of laser shots.

experimental conditions was calculated from seven replicated values [29]. Moreover, the ratio of two emission lines possessing the same upper level (or as close as possible) has been selected to ignore the effect of the plasma temperature on the variation between the ratio emission lines and their corresponding concentrations. Figure 4 shows the RSDs of ratios for (Cr I 433.49 nm/Ni I 356.63 nm), (Cr I 460.07 nm/Ni I 431.47 nm), (Nb I 378.70 nm/Ni I 394.61 nm) and (Nb I 419.08 nm/Ni I 409.36 nm) as a function of pulse energy in each laser shot. One can see the RSDs become much better with higher energies since the laser pulse is more stable at higher laser energies.

Further, the number of shots is very important due to their effects on measuring time aspects. In Fig. 5 we optimized the RSD of the ratio for (Cr I 433.49 nm/Ni I 356.63 nm), (Cr I 460.07 nm/Ni I 431.47 nm), (Nb I 378.70 nm/Ni I 394.61 nm) and (Nb I 419.08 nm/Ni I 409.36 nm) line intensities. RSD values decrease significantly and then become stable when the laser shots continuously increase.

4.2. Calibration curves

In this work, the optimized parameters of 50 shots and 150 mJ pulse energy were chosen for the calibration curves. In Fig. 6, the calibration curves of Cr/Ni and Nb/Ni are plotted. It can be noticed from Fig. 6a that the resonance line pairs of (Cr I 460.07 nm/Ni I 341.47 nm) and (Cr I 449.68 nm/Ni I 341.47 nm) have nonlinear behavior (bending) due to the self-absorption effect [9]. Moreover, the line pair of (Cr I 433.49 nm/Ni I 356.63 nm) has a straight-line trend. On the other hand, Fig. 6b shows similar characteristics of calibration lines to those of niobium of (Nb I 380.29 nm/Ni I 394.61 nm) and (Nb I 419.08 nm/Ni I 409.36 nm) which display the bending, while (Nb I 378.71 nm/Ni I 374.90 nm) has a straight line trend. However, to establish ideal calibration curves,

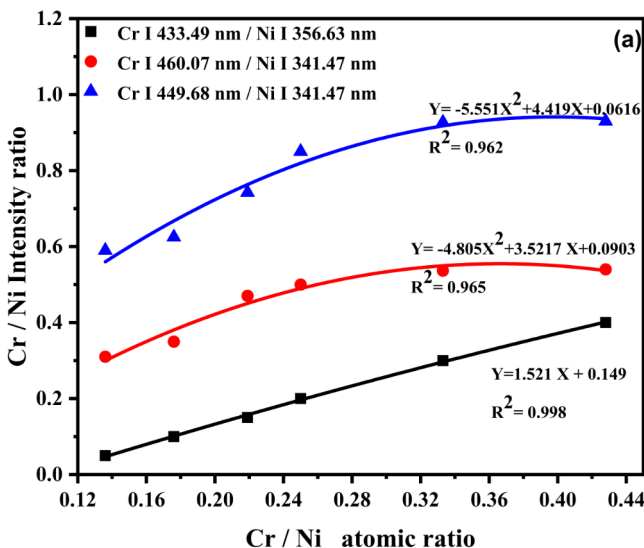


Fig. 6. Calibration curves for targeting elements Cr (a) and Nb (b) in nickel alloys.

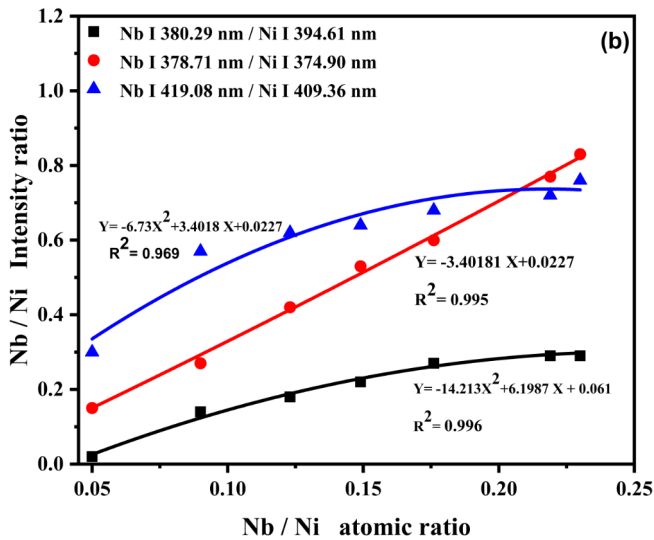


Fig. 6. Continued.

Table 3. Elemental contents [wt.%] of Cr and Nb measured by LIBS.

No.	Cr/Ni (EDS)	Cr/Ni (LIBS)	Relative error [%]
1	0.352	0.341	3.4
2	0.325	0.335	3.1
3	0.294	0.278	5.4
4	0.264	0.280	4.9
	Nb/Ni (EDS)	Nb/Ni (LIBS)	
1	0.117	0.120	2.5
2	0.147	0.156	6.1
3	0.176	0.167	5.1
4	0.205	0.219	6.8

the criteria are to choose the non-resonance line to avoid the self-absorption effect. So, we examined the emission intensity ratios of different Ni lines *versus* the atomic ratios but we selected only the linear dependences. The measurements of elemental concentrations using LIBS were close to those of EDS results with relative errors varying between (3.1 to 5.4 for Cr/Ni) and (2.5 to 6.8 Nb/Ni) as shown in Table 3.

4.3. LIBS-hardness method

The following step of our study was to correlate the emission intensity ratio of ionic chromium Cr II to atomic chromium Cr I emission lines with the Vickers mechanical hardness. The results demonstrated in Fig. 7 indicate a positive linear correlation for three different ratios of considered emission lines with different regression values in the

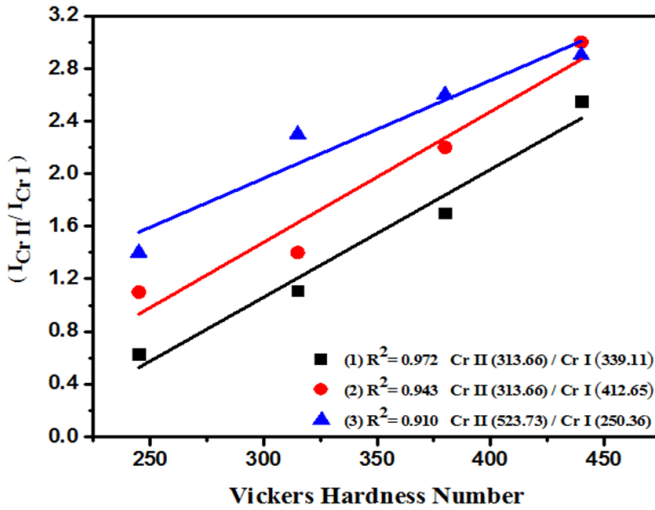


Fig. 7. Intensity ratios of ionic to atomic (Cr II/Cr I) emission lines *versus* surface hardness of Ni-Cr-Nb alloys.

range of the measured hardness. The ratio Cr II 313.66/Cr I 393.11 showed the outstanding positive linear correlation with $R^2 = 0.972$, compared with the other investigated ratios. This result confirms that the ratio of the ionic to atomic Cr II/Cr I spectral lines' emission intensity could be a valuable measurement tool for the surface hardness. This relationship with the mechanical hardness has been established in case of iron-based materials [30], cast iron samples [31] and aluminum alloy containing zeolite [32]. The behavior is interpreted in terms of laser-induced shock wave whose speed is greater for harder materials, due to the increase in a repulsive force, resulting in an enhancement of the ionization process and then of the ionic to neutral intensity ratio.

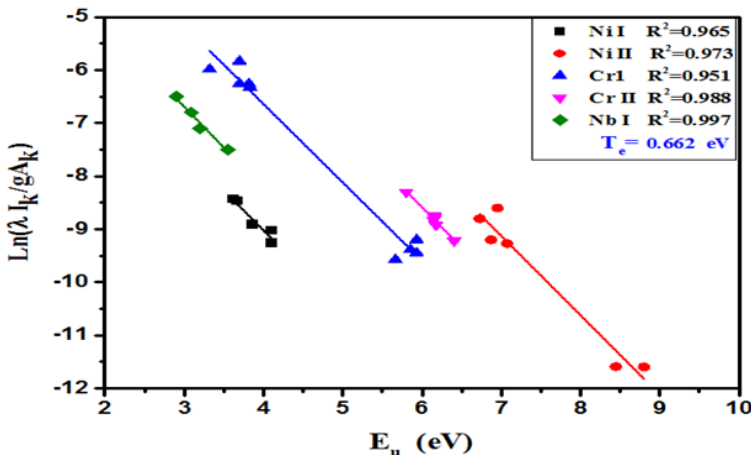


Fig. 8. Saha-Boltzmann plot of the emission lines present in sample No. 3.

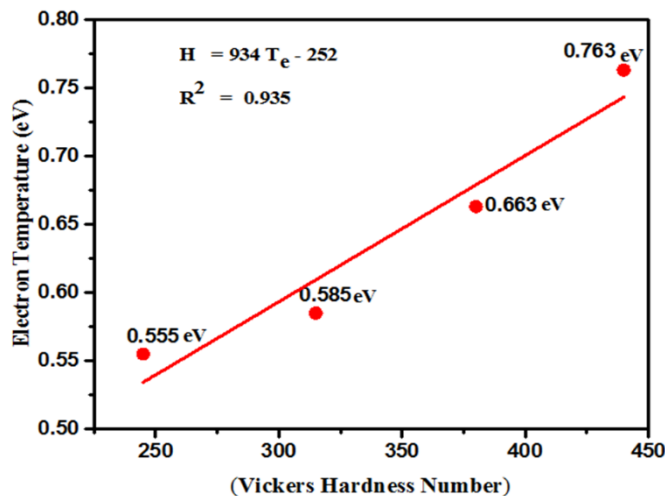
Table 4. Plasma parameters for nickel alloys samples.

No.	Sample	T_e [eV]	N_e [cm^{-3}]
1	Ni-24Cr-8Nb	0.555	8.9×10^{16}
2	Ni-22Cr-10Nb	0.585	6.8×10^{16}
3	Ni-20Cr-12Nb	0.663	3.8×10^{16}
4	Ni-18Cr-14Nb	0.763	3.1×10^{16}

In addition, the possibility of hardness measurement could be done by measuring the values of the plasma parameters, *i.e.* electron density N_e and excitation temperature T_e utilizing Eqs. (3) and (4). Plots of $\ln(\lambda I_k/gA_{ki})$ versus E_k have been drawn for five emission lines of elements (Ni I, Ni II, Cr I, Cr II and Nb I) in the spectra of sample No. 3 as shown in Fig. 8. The excitation temperatures have been calculated from the slopes of the lines ($-1/k_B T$). Also, the Ni I spectral line at 341.47 nm is used to calculate the electron number density where Stark – broadening value of $\omega_s = 0.29$ nm is substituted in Eq. (4) [33]

T_e and N_e of all considered samples are listed in Table 4. It can be seen that excitation temperature increases as thermal conductivity of sample decreases. This could be due to an increase in the amount of heat that is confined inside the sample [34].

Figure 9 demonstrates the relation between sample hardness and T_e . It was clear that the hardest sample has the highest excitation temperature, T_e increases from 0.555 to 0.763 eV corresponding to the increase in hardness from 245 to 440 VHM. This linear correlation can be written by semi-empirical formula as $HV = 934T_e - 252$. Essentially, this formula can be applied for Ni-Cr-Nb alloys evaluated at the same experimental conditions. The same trend has been previously reported by COWPE *et al.* [35] for bioceramics and by SATTAR *et al.* [16] for tungsten heavy alloys. They revealed

Fig. 9. Plasma temperature T_e with hardness.

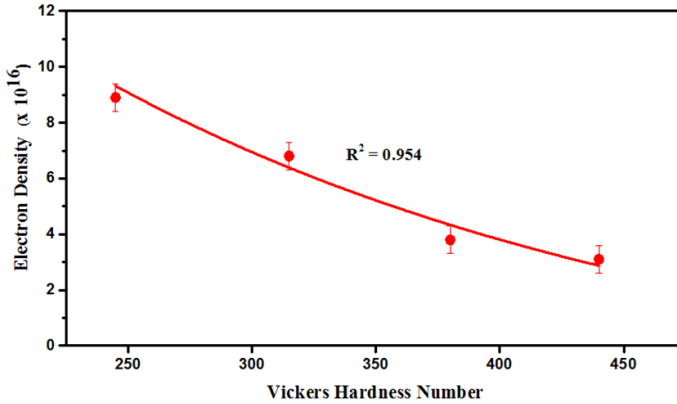


Fig. 10. Variation in electron density with surface hardness.

that the plasma shockwave velocity also influenced the value of plasma electron temperature.

Regarding the electron density, the values of N_e have inverse exponential correlation with hardness of considered alloys since they varied from 8.9×10^{16} to $3.1 \times 10^{16} \text{ cm}^{-3}$ from soft to hard alloys as shown in Fig. 10. As the electron density directly depends on the rate of ablated mass of material, and the latter is inversely related to hardness, we can conclude that N_e decreases if the materials become harder [16].

4.4. LIBS – thermal conductivity analysis

As a final step, an attempt was carried out to explore the relationship between the spectral analysis and thermal conductivity of examined alloys. Figure 11 shows the Cr I 433.99 nm, Cr I 460.07 nm, Cr I 449.68 nm and Cr I 339.45 nm line intensities as a function of measured thermal conductivity of four alloys. One can see that the behaviour is identical with a clear reverse linear correlation and different values of R^2 ; the highest value of $R^2 = 0.99$ was for Cr I 449.68 nm. This decline in line intensity is attributed to a decrease of ablated mass which should be related to the decrease in maximum temperature at the surface of materials having high thermal conductivity. Further, the two main factors which can influence the emission line intensity are T_e and N_e as it can be seen in Eq. (2). Therefore, the line intensity is directly proportionate to the concentration of free atoms in the plasma, that is, to the quantity of ablated mass M_v . Obviously from Eq. (1), the ablated mass is related directly to the laser energy E and inversely proportional to thermal properties.

On the other hand, Fig. 12 shows the variation of electron temperature with increasing thermal conductivity K . There is a linear decrease in T_e of alloys and it could be represented by a semi-empirical formula as $K = 163 - 135T_e$. The reason of T_e variation is attributed to a reduction of ablation efficiency (low ablation rates) with an increase in thermal conductivity [16]. In fact, the laser energy that reaches the bulk

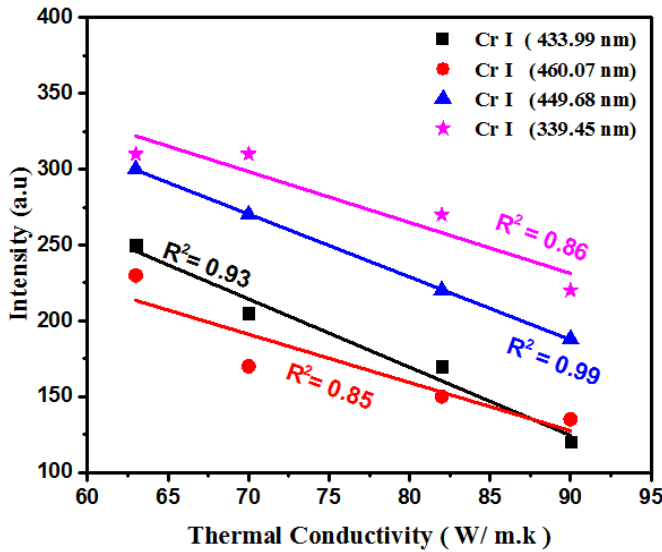


Fig. 11. Line emission intensities of Cr I 433.99 nm, Cr I 460.07 nm, Cr I 449.68 nm and Cr I 339.45 nm versus thermal conductivity.

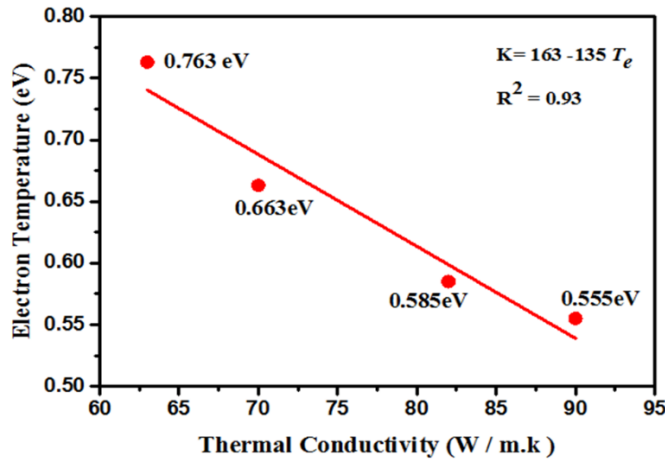


Fig. 12. Correlation between electron temperature and thermal conductivity of Ni-Cr-Nb alloys.

material generates heat, which will reside longer into the materials with a lower thermal conductivity, leading to remarkable mass removal enhancement.

5. Conclusions

This investigation underlines that LIBS can be used for the elemental composition and measurement of hardness and thermal conductivity of nickel alloys. Calibration curves

have been formed for Cr and Nb based on a group of observed lines presented in the considered alloys. Also, the spectral analysis and plasma parameters, *i.e.* plasma temperature T_e and electron density N_e , have been used to estimate surface hardness and thermal conductivity. The results obtained between the hardness and the ratio Cr II 313.66 nm/Cr I 339.11 nm showed the outstanding positive linear correlation with $R^2 = 0.972$. Experimental results indicate the positive correlation between T_e and nickel alloys hardness. Moreover, the electron temperature correlates inversely with the thermal conductivity due to the reduction of ablation efficiency. The results addressed the importance of using LIBS technique not only for the compositional analysis of nickel alloys but also for monitoring their thermal and mechanical properties.

Acknowledgements – This work was supported by the Ministry of Higher Education and Scientific Research – Iraq/Al-Nahrain University.

References

- [1] GAUDIUSO R., DELL'AGLIO M., DE PASCALE O., SENESI G.S., DE GIACOMO A., *Laser induced breakdown spectroscopy for elemental analysis in environmental, cultural heritage and space applications: a review of methods and results*, *Sensors* **10**(8), 2010, pp. 7434–7468, DOI: [10.3390/s100807434](https://doi.org/10.3390/s100807434).
- [2] LUO W.F., ZHAO X.X., ZHU H.Y., XIE D.H., LIU J., JIN P.F., *Spectral analysis of Qinling Mountain rock using laser induced breakdown spectroscopy*, *Journal of Modern Optics* **60**(21), 2013, pp. 1905–1909, DOI: [10.1080/09500340.2013.865803](https://doi.org/10.1080/09500340.2013.865803).
- [3] SENESI G.S., *Laser-induced breakdown spectroscopy (LIBS) applied to terrestrial and extraterrestrial analogue geomaterials with emphasis to minerals and rocks*, *Earth-Science Reviews* **139**, 2014, pp. 231–267, DOI: [10.1016/j.earscirev.2014.09.008](https://doi.org/10.1016/j.earscirev.2014.09.008).
- [4] GONDAL M.A., NASR M.M., AHMED Z., YAMANI Z.H., *Determination of trace elements in volcanic rock samples collected from cenozoic lava eruption sites using LIBS*, *Journal of Environmental Science and Health, Part A* **44**(5), 2009, pp. 528–535, DOI: [10.1080/10934520902720116](https://doi.org/10.1080/10934520902720116).
- [5] WANG S., TIAN D., XU M., LIN Q., WANG J., GUO G., YANG G., DUAN Y., *Elemental analysis of cemented carbides by calibration-free portable laser-induced breakdown spectroscopy*, *Instrumentation Science & Technology* **46**(3), 2018, pp. 277–291, DOI: [10.1080/10739149.2017.1380663](https://doi.org/10.1080/10739149.2017.1380663).
- [6] BULAJIC D., CRISTOFORETTI G., CORSI M., HIDALGO M., LEGNAIOLI S., PALLESCHI V., SALVETTI A., TOGNONI E., GREEN S., BATES D., STEIGER A., FONSECA J., MARTINS J., MCKAY J., TOZER B., WELLS D., WELLS R., HARITH M.A., *Diagnostics of high-temperature steel pipes in industrial environment by laser-induced breakdown spectroscopy technique: the LIBSGRAIN project*, *Spectrochimica Acta Part B: Atomic Spectroscopy* **57**(7), 2002, pp. 1181–1192, DOI: [10.1016/S0584-8547\(02\)00060-5](https://doi.org/10.1016/S0584-8547(02)00060-5).
- [7] KUZUYA M., *A sorting system for aluminum alloy scrap based on laser-induced breakdown spectroscopy*, *Science Journal of Analytical Chemistry* **7**(3), 2019, pp. 65–71, DOI: [10.11648/j.sjac.20190703.11](https://doi.org/10.11648/j.sjac.20190703.11).
- [8] VARELA J.A., AMADO J.M., TOBAR M.J., MATEO M.P., YAÑEZ A., NICOLAS G., *Characterization of hard coatings produced by laser cladding using laser-induced breakdown spectroscopy technique*, *Applied Surface Science* **336**, 2015, pp. 396–400, DOI: [10.1016/j.apsusc.2015.01.037](https://doi.org/10.1016/j.apsusc.2015.01.037).
- [9] KASHIWAKURA S., WAGATSUMA K., *Characteristics of the calibration curves of copper for the rapid sorting of steel scrap by means of laser-induced breakdown spectroscopy under ambient air atmospheres*, *Analytical Sciences* **29**(12), 2013, pp. 1159–1164, DOI: [10.2116/analsci.29.1159](https://doi.org/10.2116/analsci.29.1159).
- [10] ARARAT-IBARGUEN C., CORVALÁN C., DI LALLA N., IRIBARREN M., PÉREZ R., VICENTE E., *Application of the LIBS technique to the study of fast impurities diffusion in Zr based alloys*, *Procedia Materials Science* **8**, 2015, pp. 1004–1013, DOI: [10.1016/j.mspro.2015.04.162](https://doi.org/10.1016/j.mspro.2015.04.162).

- [11] GAUDIUSO R., UHLIR K., GRIESSER M., *Micro-invasive depth profile analysis by laser-induced breakdown spectroscopy (LIBS): the case of mercury layers on Sasanian coins*, Journal of Analytical Atomic Spectrometry **34**(11), 2019, pp. 2261–2272, DOI: [10.1039/C9JA00165D](https://doi.org/10.1039/C9JA00165D).
- [12] LI J., LU J., DAI Y., DONG M., ZHONG W., YAO S., *Correlation between aging grade of T91 steel and spectral characteristics of the laser-induced plasma*, Applied Surface Science **346**, 2015, pp. 302–310, DOI: [10.1016/j.apsusc.2015.03.186](https://doi.org/10.1016/j.apsusc.2015.03.186).
- [13] WANG S., WANG Y., LIU C., MAZUMDER J., *In-situ monitoring on micro-hardness of laser molten zone on AISI4140 steel by spectral analysis*, Scientific Reports **10**, 2020, article 4241, DOI: [10.1038/s41598-019-55559-z](https://doi.org/10.1038/s41598-019-55559-z).
- [14] LEGNAIOLI S., CAMPANELLA B., POGGIALINI F., PAGNOTTA S., HARITH M.A., ABDEL-SALAM Z.A., PALLESCHI V., *Industrial applications of laser-induced breakdown spectroscopy: a review*, Analytical Methods **12**(8), 2020, pp. 1014–1029, DOI: [10.1039/C9AY02728A](https://doi.org/10.1039/C9AY02728A).
- [15] ABDEL-SALAM Z.A., GALMED A.H., TOGNONI E., HARITH M.A., *Estimation of calcified tissues hardness via calcium and magnesium ionic to atomic line intensity ratio in laser induced breakdown spectra*, Spectrochimica Acta Part B: Atomic Spectroscopy **62**(12), 2007, pp. 1343–1347, DOI: [10.1016/j.sab.2007.10.033](https://doi.org/10.1016/j.sab.2007.10.033).
- [16] SATTAR H., RAN H., DING W., IMRAN M., AMIR M., DING H., *An approach of stand-off measuring hardness of tungsten heavy alloys using LIBS*, Applied Physics B **126**, 2020, article 5, DOI: [10.1007/s00340-019-7355-0](https://doi.org/10.1007/s00340-019-7355-0).
- [17] LABUTIN T.A., POPOV A.M., LEDNEV V.N., ZOROV N.B., *Correlation between properties of a solid sample and laser-induced plasma parameters*, Spectrochimica Acta Part B: Atomic Spectroscopy **64**(10), 2009, pp. 938–949, DOI: [10.1016/j.sab.2009.07.033](https://doi.org/10.1016/j.sab.2009.07.033).
- [18] PALANCO S., CABALIN L.M., ROMERO D., LASERNA J.J., *Infrared laser ablation and atomic emission spectrometry of stainless steel at high temperatures*, Journal of Analytical Atomic Spectrometry **14**(12), 1999, pp. 1883–1887, DOI: [10.1039/A905472C](https://doi.org/10.1039/A905472C).
- [19] DARBANI S.M.R., GHEZELBASH M., MAJD A.E., SOLTANOLKOTABI M., SAGHAFFAR H., *Temperature effect on the optical emission intensity in laser induced breakdown spectroscopy of super alloys*, Journal of the European Optical Society – Rapid Publications **9**, 2014, article 14058, DOI: [10.2971/jeos.2014.14058](https://doi.org/10.2971/jeos.2014.14058).
- [20] HAMAD T.K., JASIM A.S., SALLOOM H.T., *Characterizing laser-induced plasma generated from MgO/PVA solid targets*, Optics and Spectroscopy **127**(1), 2019, pp. 153–158, DOI: [10.1134/S0030400X19070099](https://doi.org/10.1134/S0030400X19070099).
- [21] FIKRY M., TAWFIK W., OMAR M.M., *Investigation on the effects of laser parameters on the plasma profile of copper using picosecond laser induced plasma spectroscopy*, Optical and Quantum Electronics **52**(5), 2020, article 249, DOI: [10.1007/s11082-020-02381-x](https://doi.org/10.1007/s11082-020-02381-x).
- [22] AKRAM M., BASHIR S., HAYAT A., MAHMOOD K., AHMAD R., KHALEEQ-U-RAHAMAN M., *Effect of laser irradiance on the surface morphology and laser induced plasma parameters of zinc*, Laser and Particle Beams **32**(1), 2014, pp. 119–128, DOI: [10.1017/S026303461300102X](https://doi.org/10.1017/S026303461300102X).
- [23] *NIST Atomic Spectra Database Lines Form*, https://physics.nist.gov/PhysRefData/ASD/lines_form.html (accessed June 2020).
- [24] LABUTIN T.A., POPOV A.M., SYCHEV D.N., ZOROV N.B., *Correlation between mechanical properties of aluminum alloys and characteristics of laser-induced plasma*, Proceedings of SPIE **7022**, 2008, article 70221C, DOI: [10.1117/12.804115](https://doi.org/10.1117/12.804115).
- [25] CABALIN L.M., LASERNA J.J., *Experimental determination of laser induced breakdown thresholds of metals under nanosecond Q-switched laser operation*, Spectrochimica Acta Part B: Atomic Spectroscopy **53**(5), 1998, pp. 723–730, DOI: [10.1016/S0584-8547\(98\)00107-4](https://doi.org/10.1016/S0584-8547(98)00107-4).
- [26] ZHANG D.C., HU Z.Q., SU Y.B., HAI B., ZHU X.L., ZHU J.F., MA X., *Simple method for liquid analysis by laser-induced breakdown spectroscopy (LIBS)*, Optics Express **26**(14), 2018, pp. 18794–18802, DOI: [10.1364/OE.26.018794](https://doi.org/10.1364/OE.26.018794).

- [27] GONDAL M.A., SHEMIS M.A., KHALIL A.A.I., NASR M.M., GONDAL B., *Laser produced plasma diagnosis of carcinogenic heavy metals in gallstones*, Journal of Analytical Atomic Spectrometry **31**(2), 2016, pp. 506–514, DOI: [10.1039/C5JA00358J](https://doi.org/10.1039/C5JA00358J).
- [28] KASHIWAKURA S., WAGATSUMA K., *Rapid sorting of stainless steels by open-air laser-induced breakdown spectroscopy with detecting chromium, nickel, and molybdenum*, ISIJ International **55**(11), 2015, pp. 2391–2396, DOI: [10.2355/isijinternational.ISIJINT-2015-316](https://doi.org/10.2355/isijinternational.ISIJINT-2015-316).
- [29] WANG X., ZHANG L., FAN J., LI Y., GONG Y., DONG L., MA W., YIN W., JIA S., *Parameters optimization of laser-induced breakdown spectroscopy experimental setup for the case with beam expander*, Plasma Science and Technology **17**(11), 2015, pp. 914–918, DOI: [10.1088/1009-0630/17/11/04](https://doi.org/10.1088/1009-0630/17/11/04).
- [30] ABDEL-SALAM Z., ABDELHAMID M., KHALIL S.M., HARITH M.A., *LIBS new application: determination of metallic alloys surface hardness*, AIP Conference Proceedings **1172**(1), 2009, pp. 49–52, DOI: [10.1063/1.3250114](https://doi.org/10.1063/1.3250114).
- [31] MOMCILOVIC M., PETROVIC J., CIGANOVIC J., CVIJOVIC-ALAGIC I., KOLDZIC F., ZIVKOVIC S., *Laser-induced plasma as a method for the metallic materials hardness estimation: an alternative approach*, Plasma Chemistry and Plasma Processing **40**, 2020, pp. 499–510, DOI: [10.1007/s11090-020-10063-5](https://doi.org/10.1007/s11090-020-10063-5).
- [32] KHALIL O.M., MINGAREEV I., BONHOFF T., EL-SHERIF A.F., RICHARDSON M.C., HARITH M.A., *Studying the effect of zeolite inclusion in aluminum alloy on measurement of its surface hardness using laser-induced breakdown spectroscopy technique*, Optical Engineering **53**(1), 2014, article 014106, DOI: [10.1117/1.OE.53.1.014106](https://doi.org/10.1117/1.OE.53.1.014106).
- [33] DJENIZE S., SKULJAN L., LABAT J., BUKVIC S., KONJEVIC R., *Measured Stark widths and shifts of several NiI and NiII spectral lines*, Astronomy and Astrophysics, Supplement Series **105**, 1994, pp. 115–118.
- [34] GUO K., CHEN A., XU W., ZHANG D., JIN M., *Effect of sample temperature on time-resolved laser-induced breakdown spectroscopy*, AIP Advances **9**(6), 2019, article 065214, DOI: [10.1063/1.5097301](https://doi.org/10.1063/1.5097301).
- [35] COWPE J.S., MOOREHEAD R.D., MOSER D., ASTIN J.S., KARTHIKEYAN S., KILCOYNE S.H., CROFTS G., PILKINGTON R.D., *Hardness determination of bio-ceramics using laser-induced breakdown spectroscopy*, Spectrochimica Acta Part B: Atomic Spectroscopy **66**(3–4), 2011, pp. 290–294, DOI: [10.1016/j.sab.2011.03.007](https://doi.org/10.1016/j.sab.2011.03.007).

Received April 4, 2020
in revised form October 18, 2020